

18,13

The effect of line-by-line laser scanning on the properties of laser-induced graphene

© K.G. Mikheev, R.G. Zonov, A.V. Syugaev, D.L. Bulatov, G.M. Mikheev

Udmurt Federal Research Center, Ural Branch Russian Academy of Sciences, Izhevsk, Russia

E-mail: k.mikheev@udman.ru

Received January 17, 2022

Revised January 17, 2022

Accepted January 21, 2022

Technology of polyimide (PI) film carbonization by direct laser treatment attracts much attention due to the versatility and ease of obtaining the carbon material, laser-induced graphene (LIG), used in the creation of various sensors and functional devices. In this work LIG film structures are obtained by line-by-line scanning of a *cw* CO₂ laser beam over the surface of the PI film. The synthesized carbon film material is studied by optical and scanning electron microscopy, X-ray photoelectron spectroscopy and Raman spectroscopy. It is shown that the Raman spectra of a single LIG line and a set of overlapping LIG lines significantly differ from each other. It is found that multiple laser scanning of the PI film leads to a marked decrease in the number of defects in the LIG structure as well as to a significant decrease in the specific surface resistance of the synthesized film material. The results obtained can be used in the synthesis of LIG film structures with improved characteristics.

Keywords: laser-induced graphene, polyimide film, line-by-line laser scanning.

DOI: 10.21883/PSS.2022.05.53520.277

1. Introduction

In recent years, new wearable and wireless technologies are rapidly developed and influence both the nanosystem industry and daily life. In order to increase performance and comfort, flexible materials and various microdevices are more widely used in these areas [1–4]. Carbon materials such as graphene, graphene oxide and carbon nanotubes are widely utilized in their manufacture [5–8]. One of the most efficient carbon material production methods is carbonization of various precursors due its convenience and cost-effectiveness. Carbonization may be carried out by means of chemical, thermal and laser exposure [9–11]. among these methods, direct laser exposure has such benefits as cost-effectiveness, achievement of any desired geometrical shape of the target material and no need for special media [12,13].

Synthetic and natural polymers may be used as precursors for laser pyrolysis [7,11,14,15]. Various devices have been developed by means of laser processing of these materials. However, for mass production of microdevices, stable commercial carbon materials are required. From this perspective, polyimide (PI) is an ideal precursor for laser pyrolysis and simultaneously serves as a substrate material. PI is an easily available material that is characterized by flexibility, resistance to most of solvents and is often used for electrical and heat insulation [16]. It was a PI-film that was first used in 2014 [17] to produce a graphene film structure by line-by-line scanning with focused pulse-periodic CO₂-laser radiation that was named „laser-induced graphene“ (LIG). From that time, a lot of research publications regarding this material have been published due to its advantages for the

production of microsupercapacitors, filters, membranes, gas sensors, etc. [18–24]. In the great majority of publications, LIG was synthesized using pulse-periodic lasers that operate in various spectral bandwidths [25–27]. Pulse-periodic laser exposure of PI-film at moderately high frequencies (e.g. for CO₂-lasers about 6 kHz [28]) cannot ensure homogeneity of the synthesized LIG film structure on the film surface. Therefore, the use of *cw* CO₂-laser radiation for achievement of a more homogeneous LIG film structure is of interest. In our recent papers, we have shown that LIG may be synthesized on PI-film surface using *cw* CO₂-laser radiation [29,30]. In particular, it has been demonstrated that the LIG film structure produced using this method has a drag-effect photocurrent generation capability [31–33] in a wide spectral range from 266 nm to 1064 nm. The purpose of the research is to investigate in more detail the influence of LIG on PI-film synthesis using line-by-line scanning with *cw* CO₂-laser on LIG structure in order to achieve LIG with improved properties for the manufacture of, for example, microsupercapacitors.

2. Research targets and methods

To form LIG samples on the 100 μ m-thick- PI-film surface a laser machine generating *cw* radiation up to 40 W at 10.6 μ m. A laser beam was focused to the PI-film surface by a 51 mm lens. The focusing lens was located inside a V-shaped nozzle and blown with air flowing from the lens to the focused beam waist. This ensured the lens surface protection against contamination with PI-film laser processing products. The focused laser spot diameter

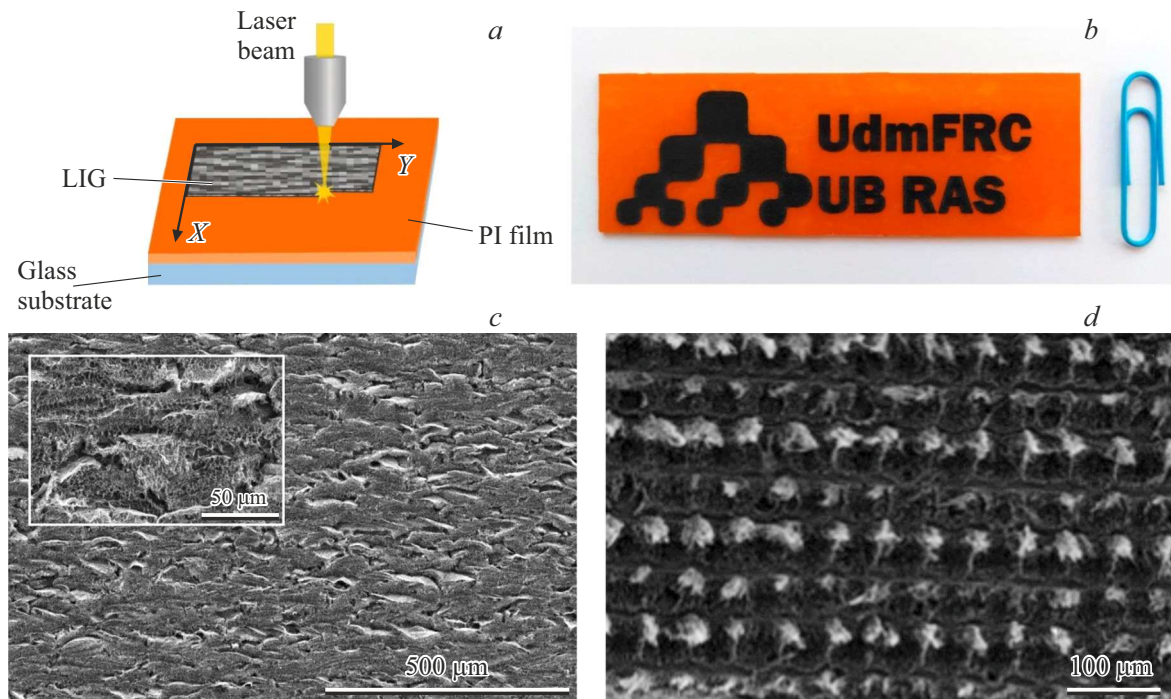


Figure 1. *a* — scheme of LIG production on a PI-film using line-by-line scanning with focused *cw* CO₂-laser radiation, *b* — photo of LIG on PI-film in a form of a logotype, *c* — typical SEM images of a LIG surface synthesized using a *cw* CO₂ laser. *d* — SEM image of a LIG surface synthesized using a pulse-periodic CO₂-laser (Reprinted from [28] with permission from Elsevier). *cw* CO₂ laser beam scanning was performed in plane *XY* with the beam moved parallel to axis *Y* from left to right, then the beam was shifted with a 25 μm increment along axis +*X*, then the laser beam was moved in the opposite direction to axis *Y* (i.e. from right to left) etc.

measured by $1/e^2$ intensity level on the PI-film was equal to 190 μm. The power of the incident radiation on the PI-film surface was varied by the laser machine power supply unit. The optimum scanning rate found during the preliminary investigations remained unchanged and was equal to 220 mm/s. For the schematic image of the laser pyrolysis process, see Fig. 1, *a*. The laser nozzle scanned, i.e. line by line went over the PI surface attached to a glass substrate, along axis *Y* and shifted after each line at 25 μm along axis *X*. The automated laser control system allowed one to achieve the LIG of free-shape. As an example, Fig. 1, *b* shows a photo of a logo of the Udmurt Federal Research Center, Urals Branch of the Russian Academy of Sciences (the organization to which the authors of this publication are affiliated), produced by LIG formation on a PI-film surface.

The sample surface morphology was characterized using Neophot 32 optical microscope coupled with ToupCam U3ISPM18000KPA (USB3.0) digital photo camera [34], and a scanning electron microscope (SEM) (Thermo Fisher Scientific Quattro S). The structure of PI-film and carbon films produced by laser exposure was analyzed using a Raman spectrometer (HORIBA HR800, excitation wavelength 632.8 nm) with laser power density of 14 kW/cm². All Raman spectra of LIG samples shown herein are given after subtraction of the luminescence background. In addition, Raman spectra of the synthesized LIG film structures

with different number of lines and scanning iterations are normalized by the D band intensity. Atomic composition and chemical bonds of films were studied using an X-ray photoelectron spectrometer (SPECS, MgK_α excitation at a constant energy analyzer transmission energy of 15 eV). Sample resistance was measured by DC measurement method at room temperature.

3. Results and discussion

Fig. 1, *c* shows the images of a LIG film surface synthesized by means of 6.2 W laser radiation using a scanning electron microscope. Fig. 1, *c* shows the lines that resemble ploughed field furrows and the inset in Fig. 1, *c* clearly shows a porous structure, with pore size up to 1 μm.

It should be noted that the LIG LIG surface structure obtained using a *cw* CO₂-laser significantly differs from the LIG surface structure obtained in [28] by means of a pulse-periodic CO₂-laser (see Fig. 1, *d*). Comparison of photographs in Fig. 1, *c, d* shows that LIG pulse-periodic *cw* laser radiation provides more homogeneous structure along the laser beam scanning line as compared with LIG synthesis using pulse-periodic laser radiation. According to the X-ray photoelectron spectroscopy data (XPS) (see Fig. 2), carbon (90.8 at.%), oxygen (7.5 at.%) and nitrogen (1.7 at.%) are present in the surface layer of the typical LIG film. The main peak in C1s spectrum is associated

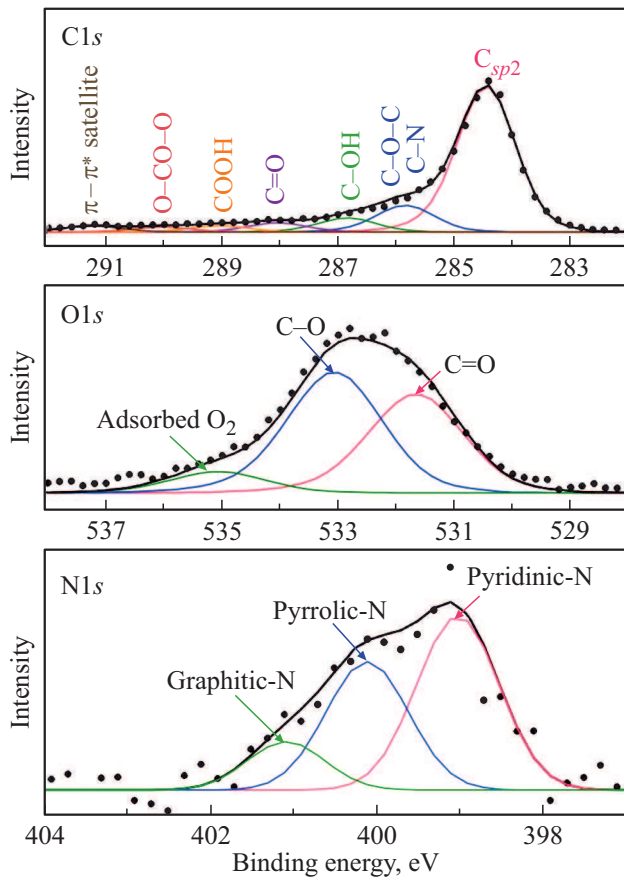


Figure 2. C1s-, O1s- and N1s-spectra of laser-induced graphene with indication of most probable spectral components obtained using an X-ray photoelectron spectrometer. An oxide-free sp^2 -carbon (with bond energy 284.4 eV) content is 68.5%.

with unfunctionalized graphene carbon with a bond energy of 284.4 eV. The high-energy portion of the spectrum is associated with the presence of various oxygen-containing groups, including ether, phenol, carbonyl, carboxyl and carbonate groups, and of C-N bonds. In O1s spectrum, components from groups with double and single bonds between carbon and oxygen atoms and a small component at 535.0 eV that may be attributed to the surface adsorbed oxygen are observed. In N1s-spectrum, components from pyridine, pyrrole and substituting (graphite-like) type nitrogen atoms, which appeared as a result of nitrogen-containing PI pyrolysis, are observed. Graphene containing such nitrogen components, is known to have a higher potential for creation of microsupercapacitors due to higher electron mobility as compared with nitrogen-free graphene [35]. XPS spectra of synthesized LIG film structures closely match the LIG research findings obtained in other papers, for example, in [36,37].

Fig. 3 shows Raman spectra of PI-film surface depending on the power of cw CO_2 -laser. The Raman spectrum of a PI-film not exposed to laser radiation shows lines that according to [38–41] may be attributed to a breathing

mode of the aromatic ring (1122 cm^{-1}), C-N stretching vibrations (1390 cm^{-1}), C=C ($\sim 1600\text{ cm}^{-1}$), and C=O (1789 cm^{-1}). It is known that when a PI film is heated up to 550°C , oxygen and nitrogen are released, when it is heated up to 700°C , carbonization takes place, and when it is heated up to 3000°C , graphenization occurs [28,42,43]. During exposure to 2 W laser radiation (Fig. 3, curve 2), PI-specific bands disappear and D (1350 cm^{-1}) and G (1590 cm^{-1}) bands appear which is indicative of the beginning of carbonization. Raman band D is caused by the defects in the hexagonal structure of sp^2 -atoms and it is absent in Raman spectra of defect-free graphite and graphene [44]. G-band is associated with the longitudinal mode of carbon atoms.

Fig. 3, curve 3 shows the Raman spectrum of a LIG obtained at 6.2 W taken at a random point on the sample surface. Increased laser exposure power obviously increases the local temperature in the area of laser radiation interaction with the PI-film and as a result 2D-band ($\sim 2660\text{ cm}^{-1}$) appears. This band is attributed to the loss of energy of a quantum of exciting radiation on excitation of excitation transverse optical vibrations of carbon atoms in graphene [45]. Narrowing of D- and G-bands and reduction of D- and G-band intensity ratio $I_{D/G}$ are also observed. Such changes in the spectrum show that graphene layers are being formed [28].

A single-layer graphene Raman spectrum is distinguished by the intense 2D-band which is fitted with one Lorentz curve with a half-width of 25 cm^{-1} , with $I_{2D}/I_G > 1$, where I_{2D} and I_G are 2D and G band intensities, respectively [44]. When the number of layers is increased, 2D-band transforms and represents itself a sum of several peaks shifted relative each other on a frequency scale. As a result, the cumulative 2D-bands width is increased and its Raman shift is increased. At the same time, its intensity as compared with G band is reduced significantly [46]. Fig. 3, curve 3 shows that 2D-band has a half-width of $\sim 45\text{ cm}^{-1}$ with $I_{2D}/I_G \approx 0.5$. It may be also noted that the Raman shift of 2D-band in the recorded Raman spectrum coincides with the that of graphene measured in [44] at 633 nm laser excitation. Thus, I_{2D}/I_G , 2D-band Raman shift and half-width show that the synthesized carbon material is composed of numerous graphene layers located in random positions with respect to each other [45,46]. Fig. 3, curve 3 show that I_D/I_G is equal to 0.5. This is indicative of the presence of defects in graphene layers [45].

It should be noted that the averaged spectrum of LIG synthesized at 6.2 W (Fig. 3, curve 4) differs from the single spectrum shown in Fig. 3, curve 3. In the averaged spectrum, $I_D/I_G \approx 1$, and the observed 2D-band is identical to 2D-band in Fig. 3, curve 3 in terms of position, intensity and width. Thus, the main difference of these spectra is in the relationship of D- and G-bands which can be explained by the structural heterogeneity of LIG. With further increase in the laser power up to 15 W, D, G and 2D band widths are also increased which is indicative of the growing number of defects in the LIG structure (see Fig. 3, curve 5). It should

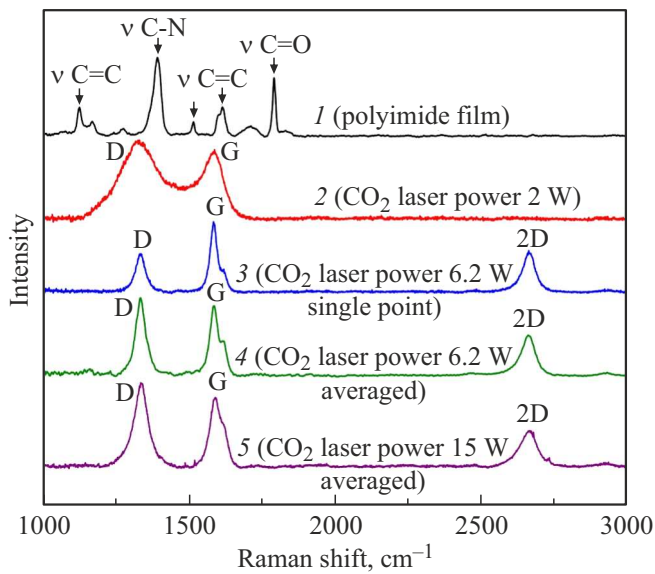


Figure 3. Raman spectra (I) in a given point of PI-film and carbon structure obtained on PI-film after (2) 2 W and (3) 6.2 W laser radiation exposure, and of carbon structure, averaged by 10 points, obtained on PI-film after (4) 6.2 W and (5) 15 W laser radiation exposure.

be noted that at this power, exfoliation of a LIG layer from the PI-substrate is observed and achievement of a stable film becomes difficult.

In all LIG spectra, D'-band ($\sim 1615 \text{ cm}^{-1}$) is present that is attributed to the double resonance scattering process [45]. This band may be indicative of the defects in graphene layers due to the presence of nitrogen demonstrated by the XPS data (see Fig. 2) [47]. The D and D' intensity ratio indicating the type of defects is ~ 3.5 which means that the defects prevail on the graphene layer edges [48]. Spectra shown in Fig. 3, (curves 2, 3 and 4) are typical of LIG [14,15,17,49,50].

Scanning with $190 \mu\text{m}$ laser beam with $25 \mu\text{m}$ increments means that the laser beam repeatedly passes the same film segment which shall obviously influence the morphology and structure of the target material. In order to investigate this, LIG samples were synthesized on the PI surface with the number of lines produced as a result of laser scanning at 6.2 W varying from one to five.

Fig. 4 shows the surface images of these samples obtained using an optical microscope and SEM cross-sectional images of the same samples. It can be seen that the LIG stripe width increases with the increase in the number of lines (it is $\sim 200 \mu\text{m}$ for single line and $\sim 300 \mu\text{m}$ for five lines). However, single line is characterized by formation of flake-like structures (see Fig. 4, a). Such flakes are clearly seen on a cross-section in Fig. 4, f. After formation of the second line, the amount of flakes is significantly reduced which is clearly seen in Fig. 4, b, g. Since each next line goes through the previous line with its larger area, this, most likely, can be single explained by the

fact that these flakes are removed by the air flow (from the laser nozzle) that protects the focusing lens against contamination. In order to investigate structural differences in LIG stripes with different number of lines, their Raman spectra were measured. The measurements were carried out across the stripe with an increment of $10 \mu\text{m}$ beginning from the edge and ending at $200 \mu\text{m}$ (the stripe width with one line) from the starting point. Such distance was chosen in order to consider the same number of points for each stripe during averaging.

Fig. 5, a shows Raman spectra (averaged by 20 measured spectra) of LIG stripes formed by line-by-line laser scanning with different number of lines. Fig. 5, a shows that a reduced number of defects in the LIG structure is observed with the increase in the number of lines. This is demonstrated by the reduction of intensity ratio of D- and G-bands (see Fig. 5, b). Thus, for the sample with single line — I_D/I_G is 2.39, while for the sample with five lines — this parameter is equal to 1.35. On the contrary, the intensity ratio of 2D-band and G-band I_{2D}/I_G grows from 0.35 to 0.42 for one and five lines, respectively. Simultaneously, D-, G-, and 2D-band half-widths are reduced (Fig. 5, c), and 2D-band Raman shift is increased with the increase in the number of lines (Fig. 5, d). All this indicates that the number of defects in graphene layers is reduced and the degree of graphenization is growing.

Such influence of the number of lines on the LIG structure can be explained as follows. During laser processing of one line on PI-film along axis Y (see Fig. 1, a), partial graphenization of the surface takes place and a stripe with a width about $200 \mu\text{m}$ (see Fig. 4, a) is formed. Then laser is shifted along axis X by $25 \mu\text{m}$ and moves along axis Y in the opposite direction. A large portion of the beam area passes over the partially graphenized layer again, thus, increasing the degree of graphenization. The next line again passes over the two previous lines with its larger area and further increases the degree of graphenization. Thus, the laser moves about 8 times over the first line area with the lowest number of intersections on the band edges. For this reason and due to the fact that the laser beam intensity is minimized on its edges, on the perimeter of an individual line we observed spectra where 2D-band is absent and wide D- and G-bands are present, i.e. amorphous carbon spectra similar to the spectrum in Fig. 3, curve 2.

Taking into account the knowledge that the repeated laser pass over the already made LIG line increases the degree of graphenization, it can be expected that the repeated laser scanning of the whole LIG sample will produce LIG with improved properties. For this, five LIG samples with different number of scanning iterations were prepared. At the first stage, all samples were scanned line by line in normal conditions, and as a result a LIG layer was formed on each sample. At the second stage, one more line-by-line laser scanning was carried out on the already made LIG layer on the four remaining samples. At the third stage, three of the previous four samples were scanned, at the

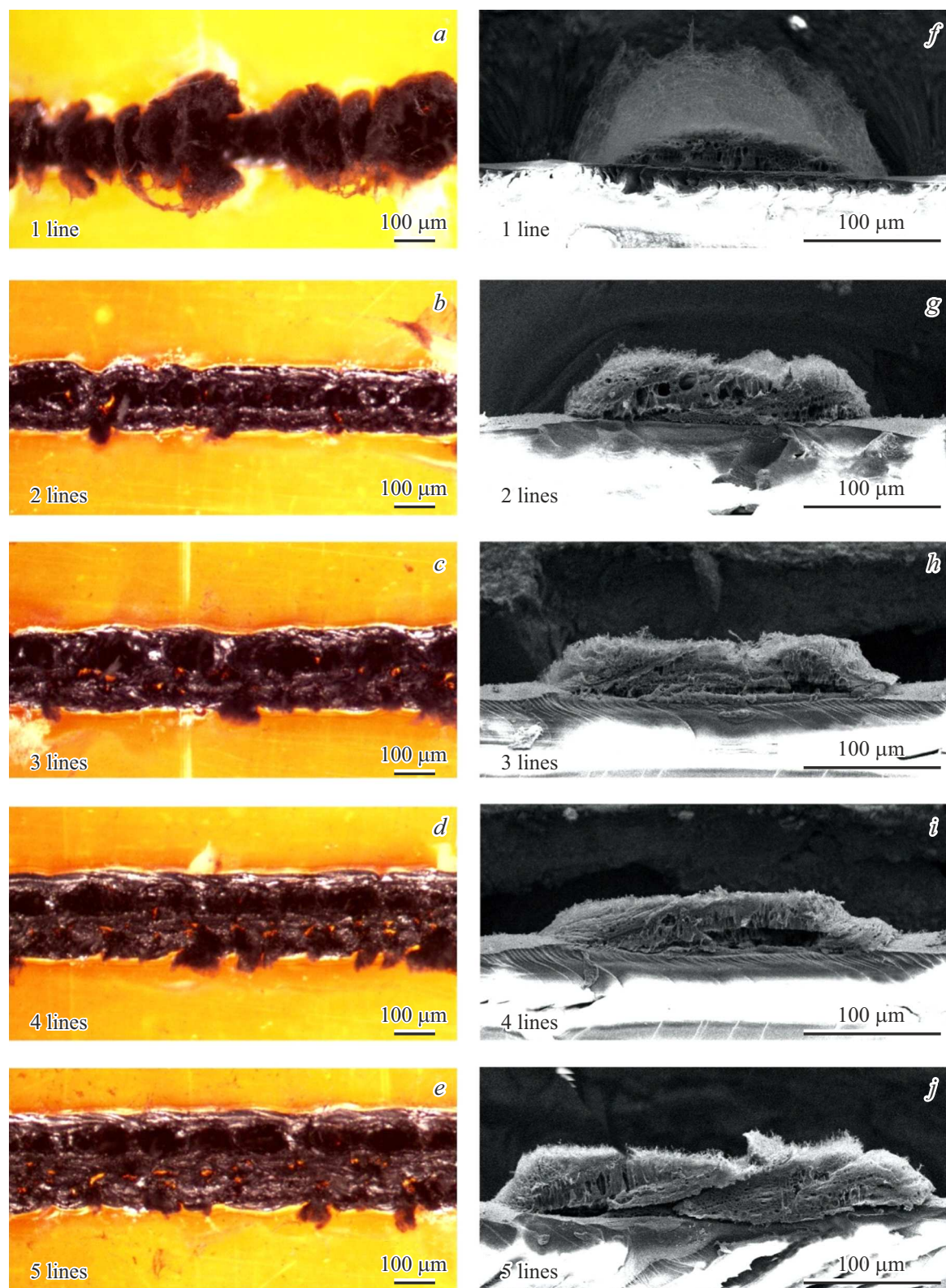


Figure 4. *a–e* — optical images of surfaces of LIG stripes formed on PI-film by means of line-by-line laser scanning with various number of lines and *f–j* — respective SEM-images of the LIG cross-section.

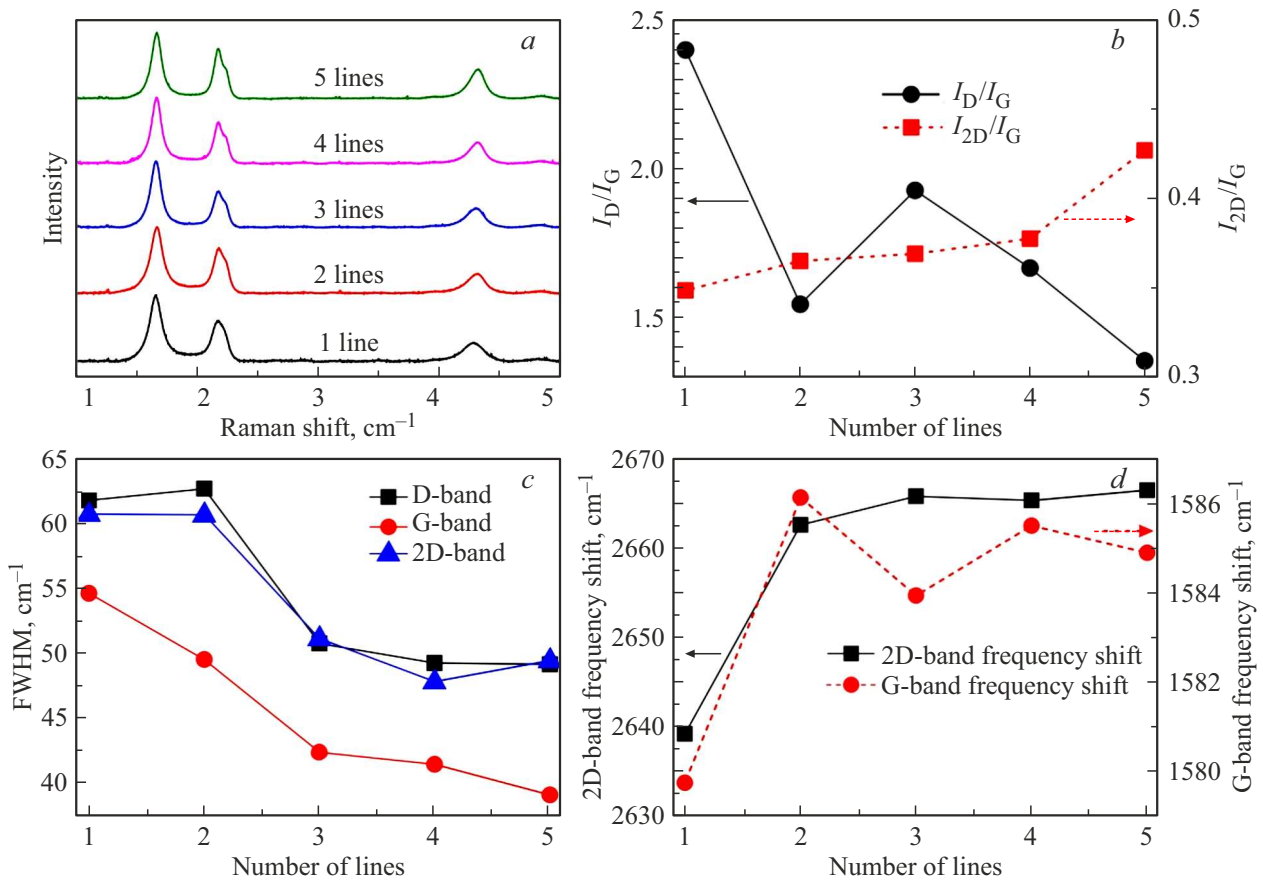


Figure 5. *a* — Raman spectra of extended LIG stripes formed by line-by-line laser scanning with the number of lines from 1 to 5, averaged by 20 spectra measured across the stripes with an increment of 10 μm . The spectra are normalized by the D-band intensity. *(b)* Intensity ratios of D- and G-bands (circles), 2D- and G-bands (squares), *(c)* half-widths (FWHM) of D-, G-, 2D-bands and *(d)* positions of G- (circles) and 2D-bands (squares) vs. the number of lines per LIG stripe.

fourth stage — two samples were scanned, and at the fifth stage — one sample was scanned. Thus, five LIG samples with different number of scanning iterations were formed: from one to five.

Fig. 6, *a* shows Raman spectra of LIG samples formed by line-by-line laser scanning with different number of laser scanning iterations averaged by 20 spectra.

It can be seen that with the increase in the number of iterations, I_D/I_G and I_{2D}/I_G are reduced (see Fig. 6, *b*). Thus, for the LIG sample produced by single scanning, $I_D/I_G = 1.06$ and $I_{2D}/I_G = 0.48$, while for the LIG sample produced by five scanning iterations, $I_D/I_G = 0.78$ and $I_{2D}/I_G = 0.34$. D-, G- and 2D-band half-widths remain approximately at the same level (see Fig. 6, *c*) and Raman shifts of G- and 2D-bands are slightly increased (see Fig. 6, *d*).

It is interesting to note that in additional experiments, when the distance between the lines was increased, the degree of surface graphenization of PI-film was decreased which is demonstrated by the increase in I_D/I_G and decrease in I_{2D}/I_G . Moreover, whatever the distance between the lines, the degree of graphenization consistently grows during the repeated laser scanning.

One of the key parameters of the LIG film structures (in terms of the development and manufacturing of electrical devices and sensors on their basis) is resistivity per square (hereinafter referred to as „sheet resistance“ R_S). Therefore, the influence of multiple laser scanning on R_S was investigated. For this, 25 samples with LIG film structure were synthesized in a form of a 0.5×3.0 cm square. The first five LIG samples were obtained by single scanning, the next group of 5 samples was obtained by double scanning, the third group of 5 samples was obtained by triple scanning, etc.

Fig. 7 shows R_S vs. the number of scanning iterations where each point was obtained after averaging of the measured sheet resistance of five samples synthesized in the same conditions. It can be seen that R_S of the LIG film structure synthesized by single laser scanning over the PI surface is equal to $29.0 \Omega/\square$. With the next scanning iterations, R_S is steadily decreased. After quintuple scanning, R_S is reduced to $21.3 \Omega/\square$, i.e. by more than 25% as compared with the value achieved by single scanning. The dependence of the LIG sheet resistance on the number of scanning iterations overall correlates with the respective I_D/I_G shown in Fig. 6, *a*, i.e. the LIG sheet resistance

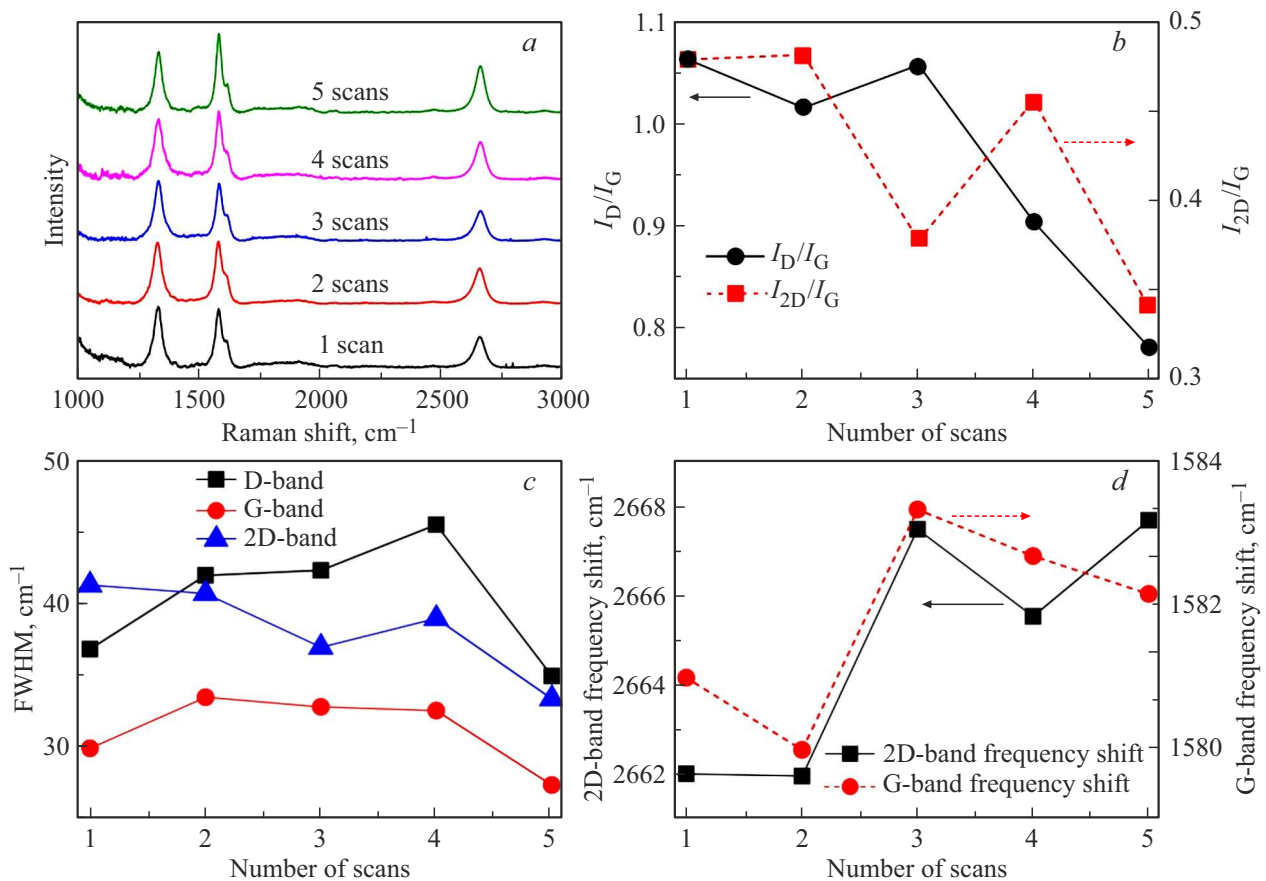


Figure 6. *a* — Raman spectra of LIG bands formed by line-by-line laser scanning with different number of laser scanning iterations averaged by 20 spectra. The spectra are normalized by D-band intensity. *(b)* Intensity ratios of D- and G-bands (circles), 2D- and G-bands (squares), *(c)* half-widths (FWHM) of D-, G-, 2D-bands and *(d)* positions of G- (circles) and 2D-bands (squares) vs. the number of laser scanning iterations.

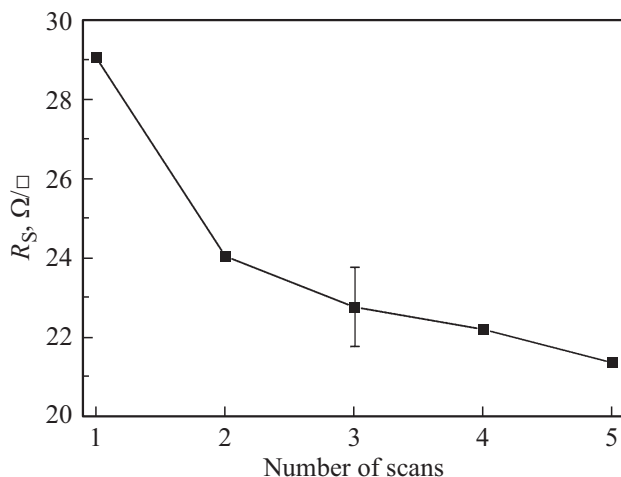


Figure 7. LIG film structure sheet resistance vs. the number of scanning iterations.

drops with the number of defects in the LIG structure. Investigations using the optical microscope and SEM show that the LIG layer thickness is increased (up to 40%) with

the increase in the number of scanning iterations, which is one of the reasons of synchronous reduction of R_S . This shall obviously influence the electrochemical properties of the synthesized LIG film structures. Investigation of such structures is of apparent interest, but is not covered herein.

4. Conclusion

The performed investigations show that PI-film pyrolysis by line-by-line scanning with 2 W focused *cw* CO₂-laser beam (waist diameter 190 μm) results in transformation of the PI-film into an amorphous carbon structure. When the power is increased up to 6.2 W, surface graphenization begins, i.e. LIG formation begins. At a higher power (> 6.2 W), LIG is also formed, however, the risk of LIG exfoliation from the PI-film is increased. Raman spectroscopy shows that the number of defects in a single LIG line is significantly greater than in the LIG stripe containing a superposition of LIG lines partially superimposing on one another (I_D/I_G is reduced from 2.39 to 1.35). Multiple laser scanning in the same segment on the PI-film surface with a specified area also reduces the number of defects in

the LIG layer (I_D/I_G is reduced from 1.06 for the LIG layer produced by single scanning to 0.78 for the LIG layer produced by quintuple scanning). It is shown that the increase in the number of laser processing iterations up to five is followed by the reduction of the sheet resistance of the synthesized LIG film structure by more than 25%. The findings may be used for further improvement of the conductive carbon structure synthesis technology for manufacture of various sensors and electronic devices.

Funding

The research has been carried out under the assignment of the Ministry of Science and Higher Education of the Russian Federation (state registration number 1021032422167-7-1.3.2) and was funded by the Russian Science Foundation (project 19-72-00071). This research has been carried out using the equipment provided by the Shared Use Center „Center of Physical and Physicochemical Methods of Analysis and Study of the Properties and Surface Characteristics of Nanostructures, Materials, and Products“ of the Udmurt Federal Research Center, Ural Branch of RAS.

Conflict of interest

The authors declare that they have no conflict of interest.

References

- [1] Y. Yang, Y. Song, X. Bo, J. Min, O.S. Pak, L. Zhu, M. Wang, J. Tu, A. Kogan, H. Zhang, T.K. Hsiai, Z. Li, W. Gao. *Nat. Biotechnol.* **38**, 217 (2020).
- [2] B. Wang, A. Facchetti. *Adv. Mater.* **31**, 1 (2019).
- [3] N. Kurra, Q. Jiang, P. Nayak, H.N. Alshareef. *Nano Today* **24**, 81 (2019).
- [4] C. Wang, C. Wang, Z. Huang, S. Xu. *Adv. Mater.* **30**, 1 (2018).
- [5] C. Zhang, Z. Peng, C. Huang, B. Zhang, C. Xing, H. Chen, H. Cheng, J. Wang, S. Tang. *Nano Energy* **81**, 105609 (2021).
- [6] V. Strauss, K. Marsh, M.D. Kowal, M. El-Kady, R.B. Kaner. *Adv. Mater.* **30**, 1 (2018).
- [7] J. Ye, H. Tan, S. Wu, K. Ni, F. Pan, J. Liu, Z. Tao, Y. Qu, H. Ji, P. Simon, Y. Zhu. *Adv. Mater.* **30**, 1801384 (2018).
- [8] Y. Zhang, L. Zhang, K. Cui, S. Ge, X. Cheng, M. Yan, J. Yu, H. Liu. *Adv. Mater.* **30**, 1 (2018).
- [9] Z. Wei, D. Wang, S. Kim, S.-Y. Kim, Y. Hu, M.K. Yakes, A.R. Laracuenta, Z. Dai, S.R. Marder, C. Berger, W.P. King, W.A. de Heer, P.E. Sheehan, E. Riedo. *Science* **328**, 1373 (2010).
- [10] S. Stankovich, D.A. Dikin, R.D. Piner, K.A. Kohlhaas, A. Kleinhammes, Y. Jia, Y. Wu, S.T. Nguyen, R.S. Ruoff. *Carbon N.Y.* **45**, 1558 (2007).
- [11] D.A. Sokolov, K.R. Shepperd, T.M. Orlando. *J. Phys. Chem. Lett.* **1**, 2633 (2010).
- [12] R. You, Y. Liu, Y. Hao, D. Han, Y. Zhang, Z. You. *Adv. Mater.* **32**, 1901981 (2020).
- [13] Z. Wan, E.W. Streed, M. Lobino, S. Wang, R.T. Sang, I.S. Cole, D.V. Thiel, Q. Li. *Adv. Mater. Technol.* **3**, 1 (2018).
- [14] R. Ye, Y. Chyan, J. Zhang, Y. Li, X. Han, C. Kittrell, J.M. Tour. *Adv. Mater.* **29**, 1702211 (2017).
- [15] R. Ye, D.K. James, J.M. Tour. *Adv. Mater.* **31**, 1803621 (2019).
- [16] D. Zhai, Y. Yang, Z. Geng, B. Cui, R. Zhao. *IEEE Trans. Terahertz Sci. Technol.* **8**, 719 (2018).
- [17] J. Lin, Z. Peng, Y. Liu, F. Ruiz-Zepeda, R. Ye, E.L.G.G. Samuel, M.J. Yacaman, B.I. Yakobson, J.M. Tour. *Nature Commun.* **5**, 5714 (2014).
- [18] Y. Ding, Z. Cheng, X. Zhu, K. Yvind, J. Dong, M. Galili, H. Hu, N.A. Mortensen, S. Xiao, L.K. Oxenløwe. *Nanophotonics* **9**, 317 (2020).
- [19] P. Zaccagnini, D. di Giovanni, M.G. Gomez, S. Passerini, A. Varzi, A. Lamberti. *Electrochim. Acta* **357**, 136838 (2020).
- [20] Y. Wang, G. Wang, M. He, F. Liu, M. Han, T. Tang, S. Luo. *Small* **2103322**, 1 (2021).
- [21] L. Huang, L. Ling, J. Su, Y. Song, Z. Wang, B.Z. Tang, P. Westerhoff, R. Ye. *ACS Appl. Mater. Interfaces* **12**, 51864 (2020).
- [22] L. Cheng, W. Guo, X. Cao, Y. Dou, L. Huang, Y. Song, J. Su, Z. Zeng, R. Ye. *Mater. Chem. Front.* (2021).
- [23] H. Wang, Z. Zhao, P. Liu, X. Guo. *Biosensors* **12**, 55 (2022).
- [24] S. Kaur, S. Karmakar, K.M. Devi, R.K. Varshney, D.R. Chowdhury. *Optik* **248**, 168073 (2021).
- [25] M.K. Smith, D.X. Luong, T.L. Bougher, K. Kalaitzidou, J.M. Tour, B.A. Cola. *Appl. Phys. Lett.* **109**, 253107 (2016).
- [26] X. Yu, N. Li, S. Zhang, C. Liu, L. Chen, S. Han, Y. Song, M. Han, Z. Wang. *J. Power Sources* **478**, 229075 (2020).
- [27] M.G. Stanford, C. Zhang, J.D. Fowlkes, A. Hoffman, I.N. Ivanov, P.D. Rack, J.M. Tour, A. Ho, I.N. Ivanov, P.D. Rack, J.M. Tour. *ACS Appl. Mater. Interfaces* **12**, 10902 (2020).
- [28] L.X. Duy, Z. Peng, Y. Li, J. Zhang, Y. Ji, J.M. Tour. *Carbon N.Y.* **126**, 472 (2018).
- [29] K.G. Mikheev, R.G. Zonov, D.L. Bulatov, A.E. Fateev, G.M. Mikheev. *Tech. Phys. Lett.* **46**, 5 (2020).
- [30] K.G. Mikheev, R.G. Zonov, T.N. Mogileva, A.E. Fateev, G.M. Mikheev. *Opt. Laser Technol.* **141**, 107143 (2021).
- [31] E.L. Ivchenko. *Optical Spectroscopy of Semiconductor Nanostructures*. Springer (2004).
- [32] G.M. Mikheev, A.S. Saushin, V.V. Vanyukov, K.G. Mikheev, Y.P. Svirko. *Nanoscale Res. Lett.* **12**, 39 (2017).
- [33] K.G. Mikheev, A.S. Saushin, R.G. Zonov, A.G. Nasibulin, G.M. Mikheev. *J. Nanophotonics* **10**, 012505 (2015).
- [34] G.M. Mikheev, R.G. Zonov, A.Yu. Popov, D.G. Kalyuzhny. *Pribory i tekhnika eksperimenta*, **46**, 3, 164 (2003) (in Russian).
- [35] E. Haque, M.M. Islam, E. Pourazadi, M. Hassan, S.N. Faisal, A.K. Roy, K. Konstantinov, A.T. Harris, A.I. Minett, V.G. Gomes. *RSC Adv.* **5**, 30679 (2015).
- [36] E.R. Mamleyev, S. Heissler, A. Nefedov, P.G. Weidler, N. Nordin, V.V. Kudryashov, K. Länge, N. MacKinnon, S. Sharma. *Npj Flex. Electron.* **3**, 2 (2019).
- [37] Z. Wan, M. Umer, M. Lobino, D. Thiel, N.T. Nguyen, A. Trinchì, M.J.A. Shiddiky, Y. Gao, Q. Li. *Carbon N.Y.* **163**, 385 (2020).
- [38] X.J. Gu. *Appl. Phys. Lett.* **62**, 1568 (1993).
- [39] D.W. Mayo, F.A. Miller, R.W. Hannah. *Course Notes on the Interpretation of Infrared and Raman Spectra*. John Wiley & Sons, Inc., Hoboken, NJ, USA (2004).
- [40] S. Devasahayam, D.J.T. Hill, J.W. Connell. *J. Appl. Polym. Sci.* **101**, 1575 (2006).
- [41] G. Socrates. *Infrared and Raman Characteristic Group Frequencies: Tables and Charts*. 3rd ed. Wiley (2004).

- [42] A. Lamberti, M. Serrapede, G. Ferraro, M. Fontana, F. Perucci, S. Bianco, A. Chiolerio, S. Bocchini. *2D Mater.* **4**, 035012 (2017).
- [43] P. Zaccagnini, C. Ballin, M. Fontana, M. Parmeggiani, S. Bianco, S. Stassi, A. Pedico, S. Ferrero, A. Lamberti. *Adv. Mater. Interfaces* **8**, 2101046 (2021).
- [44] A.C. Ferrari. *Solid State Commun.* **143**, 47 (2007).
- [45] L.M. Malard, M.A. Pimenta, G. Dresselhaus, M.S. Dresselhaus. *Phys. Rep.* **473**, 51 (2009).
- [46] A.C. Ferrari, J.C. Meyer, V. Scardaci, C. Casiraghi, M. Lazzeri, F. Mauri, S. Piscanec, D. Jiang, K.S. Novoselov, S. Roth, A.K. Geim. *Phys. Rev. Lett.* **97**, 1 (2006).
- [47] Z. Zafar, Z.H. Ni, X. Wu, Z.X. Shi, H.Y. Nan, J. Bai, L.T. Sun. *Carbon N. Y.* **61**, 57 (2013).
- [48] A. Eckmann, A. Felten, A. Mishchenko, L. Britnell, R. Krupke, K.S. Novoselov, C. Casiraghi. *Nano Lett.* **12**, 3925 (2012).
- [49] X. Wang, Y. Cui, Y. Tao, H. Yang, J. Zhao. *J. Electron. Mater.* **10**, (2020).
- [50] R. Ye, D.K. James, J.M. Tour. *Acc. Chem. Res.* **51**, 1609 (2018).